

Fluctuations of thermodynamic variables in stationary compressible turbulence

Diego A. Donzis[†] and Shriram Jagannathan

Department of Aerospace Engineering, Texas A&M University, College Station, TX 12345, USA

(Received 5 March 2013; revised 31 May 2013; accepted 19 August 2013)

A large database of new direct numerical simulations of forced compressible turbulence on up to 2048^3 grids, and a range of Reynolds (R_λ) and turbulent Mach (M_t) numbers, is analysed to study the scaling of pressure, density and temperature fluctuations. Small-perturbation analysis is used to study the scaling of variances, and different cross-correlations as well as spectra. Qualitative differences are observed between low and high M_t . The probability density functions (p.d.f.s) of pressure and density are negatively skewed at low M_t (consistent with incompressible results) but become positively skewed at high M_t . The positive tails are found to follow a log-normal distribution. A new variable is introduced to quantify departures from isentropic fluctuations (an assumption commonly used in the literature) and is found to increase as M_t^2 . However, positive fluctuations of pressure and density tend to be more isentropic than negative fluctuations. In general, Reynolds number effects on single-point statistics are observed to be weak. The spectral behaviour of pressure, density and temperature is also investigated. While at low M_t , pressure appears to scale as $k^{-7/3}$ (k is the wavenumber) in the inertial range as in incompressible flows, a $k^{-5/3}$ scaling also appears to be consistent with the data at a range of Mach numbers. Density and temperature spectra are found to scale as $k^{-5/3}$ for a range of Mach numbers.

Key words: compressible turbulence, turbulence simulation, turbulent flows

1. Introduction

A distinguishing feature of compressible turbulence is the appearance of fluctuations in thermodynamic variables. In many situations of practical and fundamental interest, it can be assumed that the flow is in thermodynamic equilibrium, in which case thermodynamic states can be determined by two thermodynamic quantities alone (Denbigh 1981). In the case of a so-called perfect gas, the relation between pressure p , density ρ , and temperature T can be explicitly written as

$$p = \rho RT, \quad (1.1)$$

where R is the gas constant of the particular fluid under consideration.

When the flow is turbulent, both hydrodynamic as well as thermodynamic variables exhibit nonlinear fluctuations in time and space over a range of scales which increases with the Reynolds number. Further, these fluctuations are expected to depend on the

[†] Email address for correspondence: donzis@tamu.edu

level of compressibility in the flow, which is typically quantified by the turbulent Mach number. Under the assumption of local and instantaneous thermal equilibrium, (1.1) has been extensively used to study a number of compressible turbulent flows numerically and experimentally (Lele 1994; Smits & Dussauge 2006; Pirozzoli 2011). The importance of understanding both mean and fluctuating parts of thermodynamic variables is well known as they play a major role in energy exchanges between kinetic and internal energy, in the overall dynamics in wall-bounded flows, and sound generation, among others.

To understand a fluctuating quantity, g , it is useful to use Reynolds decomposition which splits g into mean and fluctuating parts, $g = \langle g \rangle + g'$ where $\langle g' \rangle = 0$. Here angular brackets $\langle \cdot \rangle$ denote a suitable ensemble average. An obvious consequence of the Reynolds decomposition of (1.1) is that mean quantities are not related according to an analogue of (1.1):

$$\langle p \rangle \neq R \langle \rho \rangle \langle T \rangle. \quad (1.2)$$

While departures are expected to be small in some circumstances, it is also expected that the degree of the discrepancy will depend on both Reynolds and Mach numbers. Similar considerations apply to the fluctuating parts. Furthermore, these fluctuations occur over a wide range of spatial and temporal scales. Thus, an important aspect of this phenomenon, as well as many other multiscale phenomena, is the distribution of energy across these scales, typically quantified using power spectra.

Our main objective here is to study the nature of pressure, density and temperature fluctuations as well as their interrelation, with an emphasis on the scaling with the Taylor Reynolds number $R_\lambda \equiv \langle \rho \rangle u' \lambda / \mu$ (u' is the root mean square (r.m.s.) of a velocity component, $\lambda \equiv u' / \langle (\partial u / \partial x)^2 \rangle^{1/2}$ is the Taylor microscale, and μ is the mean viscosity) and the turbulent Mach number $M_t = \langle u_i u_i \rangle^{1/2} / c$ (c is the mean speed of sound and summation is implied). For this we have generated a large database of direct numerical simulations (DNS) of isotropic compressible turbulence.

There have been numerous studies investigating different aspects of the effects of compressibility on turbulence using DNS in decaying flows (Lee, Lele & Moin 1991; Sarkar *et al.* 1991; Kida & Orszag 1992; Samtaney, Pullin & Kosovic 2001; Pirozzoli & Grasso 2004; Lee & Girimaji 2011) and forced flows (Kida & Orszag 1990; Petersen & Livescu 2010; Wang *et al.* 2011, 2012). A general conclusion from these studies is that the evolution of some variables depends significantly on initial conditions or forcing schemes. In particular, the decaying cases show that quantities such as dilatation or pressure–dilatation correlation present a strong dependence on the initial degree of compressibility as well as on thermodynamic fluctuations while others, such as turbulent kinetic energy, possess only a weak dependence on them. For forced flows, while the statistics depend on whether the forcing is solenoidal or dilatational, the long-term statistics seem independent of initial conditions. This kind of flow is our main interest here. Similar conclusions apply to shear flows (Blaisdell, Mansour & Reynolds 1993), where it has also been suggested that this weak dependence on initial conditions may cause modelling of forced flows to be more amenable to analytical treatment. Specifically, our forcing scheme is purely solenoidal and applied to the momentum equation (described in §2), which allows us to investigate fluctuations of thermodynamic variables as a result of Navier–Stokes dynamics exclusively, leaving the effect of dilatational forcing for future investigations.

Unlike previous work, our focus is on a systematic study of the scaling of the fluctuating thermodynamic variables and their mutual relation as a result of the equation of state (1.1) at a wide range of Reynolds and Mach numbers,

using simulations at unprecedented resolutions. In addition to the importance of studying the Reynolds and Mach number scaling of low-order moments such as the variance of thermodynamic variables (Lele 1994; Smits & Dussauge 2006), there is also interest in more complete descriptions of these variables. For example, while the probability density function (p.d.f.) of pressure is negatively skewed in incompressible flows (Pumir 1994), as the turbulent Mach number increases and fluctuations become stronger, this asymmetry cannot be sustained for arbitrarily large fluctuations in compressible flows, since pressure, being a positive quantity, requires bounded negative fluctuations. There has also been interest in the statistics of density fluctuations, as they are related, for example, to the process of star formation and development of hierarchical structures (Scalo *et al.* 1998). In particular, the scaling of the variance of density with the Mach number seems to be of particular relevance, along with the specific form of the entire p.d.f. (Federrath, Klessen & Schmidt 2008). It has been suggested, based on different assumptions, that the p.d.f. of density should obey log-normal statistics (Blaisdell *et al.* 1993) even in isothermal flows (Padoan, Jones & Nordlund 1997; Beetz *et al.* 2008; Federrath *et al.* 2008). However, this has not been studied systematically for fully turbulent non-isothermal flows at a range of Reynolds and Mach numbers. As we show below, log-normality is indeed observed, though only for positive fluctuations. Negative fluctuations are wider than log-normal but they narrow as the Mach number increases, indicating a possible log-normal behaviour for the entire p.d.f. at very high M_t .

The specific relation between different thermodynamic variables in turbulent flows is also of great interest, particularly for turbulence modelling. In a number of theoretical approaches aimed at understanding compressible turbulence (e.g. Chandrasekhar 1951; Kraichnan 1953; Erlebacher *et al.* 1990), fluctuations are taken to be isentropic due to the significant analytical simplifications that result from such an assumption. However, it is not clear, *a priori*, to what degree such an assumption is justified. As we show below, while departures from isentropic behaviour grow with M_t , positive fluctuations of density and pressure, for example, tend to be more isentropic than negative fluctuations.

In addition to single-point statistics which provide important information about the nature of random processes in general, one is also interested in the spatial structure of the fluctuations. Thus, it is also common to study the power spectrum of these variables. Classical phenomenology for incompressible flows (Monin & Yaglom 1975) suggests universality at small scales with a $k^{-7/3}$ inertial-range scaling (k is the wavenumber) for the pressure spectrum, which has indeed been observed in simulations (Gotoh & Fukayama 2001) and experiments (Tsuji & Ishihara 2003). Similar scaling is thus expected for compressible flows at low M_t . However, in order to assess inertial-range scaling, high Reynolds numbers are needed, in which case simulations may become computationally extremely expensive. With current computational power it is now possible to assess some of these issues, as we show below. Density spectra have also been extensively studied, though mainly in astrophysical contexts where the flow is typically treated as isothermal (e.g. Dastgeer & Zank 2005). However, little is known about the Reynolds and Mach number scaling of density spectra in non-isothermal flows, especially at high R_λ . A similar situation exists for temperature spectra, which have rarely been studied in fully compressible turbulence. The challenge here is, again, the need to achieve Reynolds numbers high enough to observe inertial-range scaling at a range of Mach numbers. As we show here, our largest simulations support a $k^{-5/3}$ scaling for density and temperature, which can be explained by the nature of temperature fluctuations assumed to be passively

advected by the flow. A general polytropic relation between thermodynamic variables is shown to result in $k^{-5/3}$ scaling for all of them.

The rest of the paper is organized as follows. In § 2 we describe the DNS database, the numerical method, and the forcing used in the present work. In § 3 we present results on the Reynolds and Mach number scaling of statistics of pressure, density, and temperature fluctuations including moments and p.d.f.s. The isentropic assumption and the support (or lack thereof) from DNS data is discussed in § 4. The focus of § 5 is on the scaling of spectra of thermodynamic variables. Conclusions are offered in § 6.

2. Numerical methods and database

The DNS code solves the fully compressible Navier–Stokes equations with variable viscosity (power-law in temperature with exponent 0.5 and constant Prandtl number, $Pr = 0.72$) using tenth-order compact schemes in space and third-order Runge–Kutta in time. The code has been scaled to hundreds of thousands of processors (Jagannathan & Donzis 2012). The forcing scheme is stochastic and applied at large scales using Gaussian random processes with finite-time correlation following that of Eswaran & Pope (1988) for incompressible flows. Mathematically, an additional term is included in the momentum equation of the form

$$\mathbf{f} = \sum_{|\mathbf{k}| < k_F} \hat{\mathbf{f}}_{\perp}(\mathbf{k}) e^{-i\mathbf{k}\cdot\mathbf{x}}, \quad (2.1)$$

where $\hat{\mathbf{f}}_{\perp}(\mathbf{k}) = \mathbf{P} \cdot \hat{\mathbf{f}}(\mathbf{k})$ with $\mathbf{P} = \mathbf{I} - \mathbf{k}\mathbf{k}/k^2$ being the standard projection operator onto a plane perpendicular to \mathbf{k} to ensure that forcing is purely solenoidal. The three-dimensional complex vector $\hat{\mathbf{f}}(\mathbf{k})$ is constructed using six independent integrated Ornstein–Uhlenbeck random processes. Unlike white noise, these processes have the property of being differentiable and, furthermore, possess a finite-time correlation. The actual energy input is the result of the correlation between the forcing and the velocity vector $\langle \mathbf{f} \cdot \mathbf{u} \rangle$ which is obtained by dotting the momentum equations with the velocity vector. Energy is removed from the system uniformly (via the energy equation) so that the mean temperature remains constant. The forcing parameters are chosen such that target Reynolds and Mach numbers are attained with integral length scales being about a fifth of the domain while the ratio of grid spacing and Kolmogorov scale ($\eta \equiv (v^3/\langle \epsilon \rangle)^{1/4}$) is always less than 2. Consistent with other studies (Petersen & Livescu 2010), grid convergence tests (to be published elsewhere) show that this resolution is enough to yield grid insensitive results. A summary of the DNS parameters is shown in table 1. We have also included the ratio of dilatational kinetic energy K_d to the total kinetic energy K which is a measure of the importance of compressibility at large scales (Kida & Orszag 1990). While K_d/K grows with M_r , it is always below $\sim 5\%$ for all the cases presented here. The skewness of the longitudinal velocity gradient, which is related to the nonlinear energy transfer, has been found to be consistent with incompressible results (Sreenivasan & Antonia 1997) with a value between -0.45 and -0.6 for all cases.

3. Single-point statistics of thermodynamic variables

As highlighted in (1.2), the mean pressure is not determined by the mean density and mean temperature alone. Instead, by taking the mean of (1.1) we find

$$\langle p \rangle = R \langle \rho T \rangle = R[\langle \rho \rangle \langle T \rangle + \langle \rho' T' \rangle], \quad (3.1)$$

N^3	R_λ	M_t	$\langle p^{*2} \rangle^{1/2}$	$\langle \rho^{*2} \rangle^{1/2}$	$\langle T^{*2} \rangle^{1/2}$	$\langle \rho^* T^* \rangle^{1/2}$	K_d/K
64^3	39	0.10	0.0048	0.0037	0.0013	0.0019	0.0000
64^3	32	0.20	0.0196	0.0154	0.0054	0.0077	0.0002
64^3	33	0.28	0.0404	0.0308	0.0114	0.0167	0.0024
64^3	38	0.39	0.0867	0.0652	0.0248	0.0369	0.0110
64^3	34	0.59	0.2056	0.1518	0.0594	0.0876	0.0388
128^3	63	0.09	0.0040	0.0032	0.0012	0.0015	0.0000
128^3	54	0.22	0.0218	0.0169	0.0061	0.0088	0.0004
128^3	60	0.29	0.0626	0.0460	0.0178	0.0273	0.0132
128^3	65	0.38	0.0991	0.0728	0.0281	0.0430	0.0245
128^3	58	0.58	0.2021	0.1479	0.0580	0.0872	0.0440
256^3	104	0.10	0.0039	0.0030	0.0011	0.0016	0.0000
256^3	101	0.20	0.0189	0.0144	0.0054	0.0079	0.0007
256^3	103	0.33	0.0630	0.0466	0.0180	0.0273	0.0108
256^3	107	0.40	0.0887	0.0658	0.0255	0.0384	0.0138
256^3	100	0.61	0.2167	0.1570	0.0623	0.0943	0.0491
512^3	173	0.10	0.0039	0.0030	0.0011	0.0016	0.0000
512^3	173	0.21	0.0180	0.0136	0.0051	0.0075	0.0001
512^3	163	0.31	0.0562	0.0413	0.0162	0.0245	0.0100
512^3	161	0.56	0.1834	0.1324	0.0527	0.0807	0.0396
1024^3	268	0.33	0.0462	0.0345	0.0136	0.0198	0.0021
2048^3	430	0.31	0.0381	0.0283	0.0111	0.0165	0.0009

TABLE 1. DNS parameters: number of grid points (N^3), Reynolds and turbulent Mach numbers (R_λ , M_t), and normalized standard deviation of pressure, density, and temperature as well as the covariance between density and temperature (see text). K_d/K is the ratio of dilatational kinetic energy to total kinetic energy.

or

$$\frac{\langle p \rangle}{R\langle \rho \rangle \langle T \rangle} = 1 + \frac{\langle \rho' T' \rangle}{\langle \rho \rangle \langle T \rangle} = 1 + \langle \rho^* T^* \rangle, \quad (3.2)$$

where the superscript $*$ is used to denote fluctuations normalized by the mean ($\rho^* = \rho' / \langle \rho \rangle$, $T^* = T' / \langle T \rangle$). Equation (3.2) shows that the inequality in (1.2) is due to a term involving density and temperature fluctuations. As an aside we note that (3.1) can also be written in a more compact form using so-called Favre (or mass-weighted) averages as $\langle p \rangle = R\langle \rho \rangle \tilde{T}$ (where the tilde represents a Favre average). However, this does not allow us to analyse the different contributions that result from various correlations involving density, and would thus not be used here.

In figure 1 we show the mean pressure normalized as in (3.2) as a function of the turbulent Mach number for all Reynolds numbers. At low M_t , the mean pressure can be accurately represented by the mean density and temperature. However, as M_t increases, departures are apparent due to the correlation between ρ' and T' . Reynolds number effects are seen to be very weak.

Equation (1.1) can also be used to obtain expressions for higher-order moments. For example, by applying Reynolds decomposition, and subtracting (3.2), we obtain an equation for pressure fluctuations, $p' = R[\rho' \langle T \rangle + \langle \rho \rangle T' + \rho' T' - \langle \rho' T' \rangle]$. Squaring this

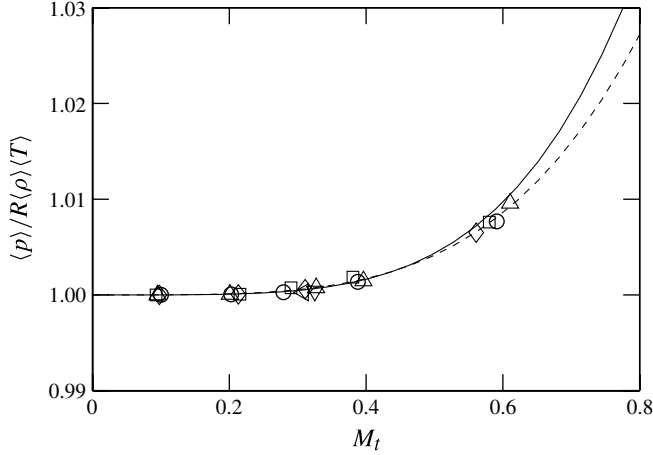


FIGURE 1. Mean pressure $\langle p \rangle$ normalized by mean density and temperature. The symbols correspond to $R_\lambda \approx 38$ (\circ), 60 (\square), 100 (\triangle), 170 (∇), 270 (\diamond), and 430 (\triangleleft). The solid and dashed lines are $1 + (M_t/1.72)^{4.5}$ and $1 + (M_t/1.97)^4$, respectively (see text).

result, averaging and normalizing by $(R\langle\rho\rangle\langle T\rangle)^2$ yields an expression for the pressure variance:

$$\frac{\langle p'^2 \rangle}{(R\langle\rho\rangle\langle T \rangle)^2} = \langle \rho^{*2} \rangle + \langle T^{*2} \rangle + 2\langle \rho^* T^* \rangle + 3\langle \rho^* T^{*2} \rangle + \langle \rho^{*2} T^{*2} \rangle + 2\langle \rho^{*2} T^* \rangle + 2\langle \rho^* T^{*2} \rangle. \quad (3.3)$$

If fluctuations are small, high-order terms (the last four terms) are expected to be negligible. More formally, we can expand (1.1) about the mean state using a Taylor series, $\langle p \rangle + p' = R\langle\rho\rangle\langle T \rangle + (\partial p/\partial\rho)\rho' + (\partial p/\partial T)T' + (\partial^2 p/\partial\rho\partial T)\rho'T' + \dots$, where derivatives are evaluated at the mean temperature and density. We can now use this result with (3.2), keep only leading-order terms, square the expression and average, to obtain

$$\frac{\langle p'^2 \rangle}{(R\langle\rho\rangle\langle T \rangle)^2} \approx \langle \rho^{*2} \rangle + \langle T^{*2} \rangle + 2\langle \rho^* T^* \rangle, \quad (3.4)$$

consistent with the first terms in (3.3).

In figure 2 we show all the terms in (3.4) (also included in table 1). In incompressible flows it is well established that $\langle p'^2 \rangle^{1/2} \approx A\langle\rho\rangle u^2$, where u' is typically taken as the root mean square of one velocity component and $A \approx 0.92$ from DNS data (Donzis, Sreenivasan & Yeung 2012). Using the mean speed of sound $\langle c \rangle = \langle \sqrt{\gamma RT} \rangle \approx \sqrt{\gamma \langle p \rangle / \langle \rho \rangle}$, with γ being the ratio of specific heats (we have assumed $\langle \sqrt{T} \rangle \approx \sqrt{\langle T \rangle}$), we can normalize the pressure variance as in (3.4) to obtain

$$\frac{\langle p'^2 \rangle}{(R\langle\rho\rangle\langle T \rangle)^2} \approx \frac{A^2 \gamma^2}{9} M_t^4, \quad (3.5)$$

where the factor 9 appears because M_t is defined using the magnitude of the velocity vector instead of a single component. This expression is compared with DNS in figure 2(a) as a dot-dashed line which is seen to be slightly below the data. A value of $A = 1.2$ represents the DNS more accurately, especially if only data at $M_t \gtrsim 0.3$

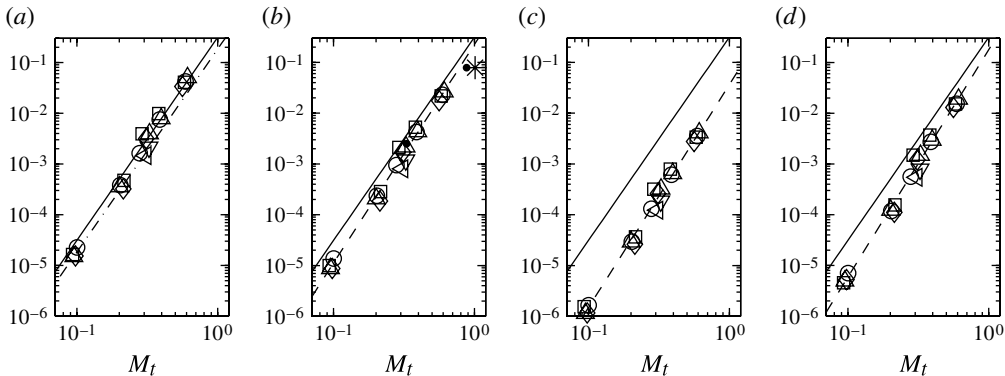


FIGURE 2. Terms in (3.4): (a) $\langle p'^2 \rangle / (R \langle \rho \rangle \langle T \rangle)^2$, (b) $\langle \rho'^2 \rangle$, (c) $\langle T'^2 \rangle$, (d) $2 \langle \rho'^* T'^* \rangle$. The symbols for different Reynolds numbers are as in figure 1; the solid lines correspond to (3.5) with $A = 1.2$ for comparison; the dot-dashed line in (a) is (3.5) with $A = 0.92$ from Donzis *et al.* (2012); the dashed lines are best-fit power laws; the black dots and the asterisk in (b) correspond to data from Kida & Orszag (1990) and Wang *et al.* (2012), respectively.

are considered. A closer look, however, reveals that the dependence on M_t is slightly steeper than that suggested by (3.5) with a best-fit exponent of 4.4. This departure from incompressible scaling appears to indicate compressibility corrections to the pressure variance. Indeed, we have inspected the ratio of variances of ‘incompressible’ pressure (obtained from the standard Poisson equation using the solenoidal velocity field) and ‘compressible’ pressure (the difference between pressure and its solenoidal component) and found a decrease from $O(100)$ at the lowest $M_t \approx 0.1$ to about $O(1)$ for $M_t \geq 0.4$.

Figures 2(b)–2(d) show the three terms on the right-hand side of (3.4), where we also include (3.5) to compare the relative contribution of the different components. Density fluctuations (figure 2b) comprise the dominant term in the expression for pressure variance. Figure 2(b) also includes data from Kida & Orszag (1990) and Wang *et al.* (2012), two DNS investigations with different forcing schemes and Reynolds numbers. The scaling and magnitude of the fluctuations appear to be relatively consistent across these DNS data. This is interesting, especially taking into account that the simulations of Kida & Orszag (1990) were not in a stationary state as no energy was removed from the system.

While temperature fluctuations (figure 2c) are an order of magnitude smaller than density, the covariance between them (the last term in (3.4)) represents a non-negligible contribution to the pressure variance. This can also be seen in figure 3 where ratios of the different contributions to pressure are shown. Density and density-temperature fluctuations appear to approach a constant at higher M_t . Temperature variance, on the other hand, remains a constant fraction of pressure variance for the entire range of Mach numbers. This constant, as well as the asymptotic states above, are discussed in § 4. For all cases, the Reynolds number effects appear to be negligible.

Just as with pressure fluctuations, the Mach number scaling of the different contributions in (3.4) is slightly steeper than M_t^4 suggested by (3.5). Best-fit exponents for density, temperature and density-temperature fluctuations over the entire range of M_t are 4.3, 4.4 and 4.5, respectively. The scaling of $\langle \rho'^* T'^* \rangle$ can be used in (3.2) for the

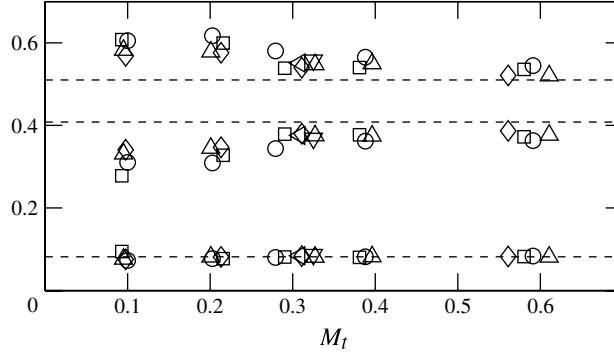


FIGURE 3. Ratios (from top to bottom) $\langle \rho^{*2} \rangle / X$, $2\langle \rho^* T^* \rangle / X$, and $\langle T^{*2} \rangle / X$ with $X = \langle p'^2 \rangle / (R(\rho) \langle T \rangle)^2$. The symbols for different Reynolds numbers are as in figure 1. The dashed lines are isentropic relations (§ 4) $1/\gamma^2$, $2(\gamma - 1)/\gamma^2$, and $(\gamma - 1)^2/\gamma^2$ (from top to bottom).

mean pressure. The result is also shown in figure 1. The difference made by using an exponent of 4 or 4.5 is seen to be small but may be relevant at higher Mach numbers.

For many fluctuating quantities, the mean value and variance provide only partial information about the nature of the fluctuations, especially those that are far from the mean. A more complete description of fluctuations at all levels is contained in the p.d.f. It is known that in incompressible turbulence, the p.d.f. of pressure fluctuations, f_p , is negatively skewed with the positive tail being close to Gaussian (Pumir 1994; Vedula & Yeung 1999). In figure 4(a) we show this p.d.f. at $R_\lambda \approx 100$ and various turbulent Mach numbers. At the lowest $M_t \approx 0.1$, the p.d.f. is consistent with incompressible results. As M_t increases, however, the p.d.f. narrows on the negative side to become slightly sub-Gaussian, and widens on the positive side. This suggests a qualitative difference between compressible and incompressible flows, namely, the increased probability of relatively large pressures (positive fluctuations) in the former as M_t increases, compared to relatively low pressures (negative fluctuations) in the latter. A plausible explanation for this shift is that pressure is a positive quantity, which implies that fluctuations are necessarily bounded from below according to $p' > -\langle p \rangle$. Thus, the increase in the intensity of pressure fluctuations with M_t (figure 2) must come from positive fluctuations where such constraint does not exist. The skewness towards the positive tail is then expected at high M_t . In general, Reynolds number effects are much weaker, as seen in figure 4(b) where f_p is shown for different Reynolds numbers at the highest M_t available.

A more quantitative measure of the asymmetry seen in the p.d.f. is the skewness factor $S_p \equiv \langle p'^3 \rangle / \langle p'^2 \rangle^{3/2}$, shown in figure 5(a). At the lowest M_t , S_p is close to -1 consistent with incompressible flows (Cao, Chen & Doolen 1999; Vedula & Yeung 1999) but increases to values close to 0.5 at $M_t \approx 0.6$. At low and high M_t , the Reynolds number effect is seen to be very weak, consistent with figure 4(b). Between $M_t \approx 0.3$ and 0.4, however, which corresponds to the transition where S_p changes sign, the data present more scatter. Because the Reynolds number trend is not monotonic at this M_t , this seems to be a reflection of the well-known statistical difficulties in computing odd-order moments of symmetric fluctuations.

Long p.d.f. tails are generally associated with large fluctuations and high flatness factors, making the latter a suitable indicator of the nature of intense fluctuations and departures from Gaussianity. In figure 5(b) we show $F_p \equiv \langle p'^4 \rangle / \langle p'^2 \rangle^2$, the flatness of

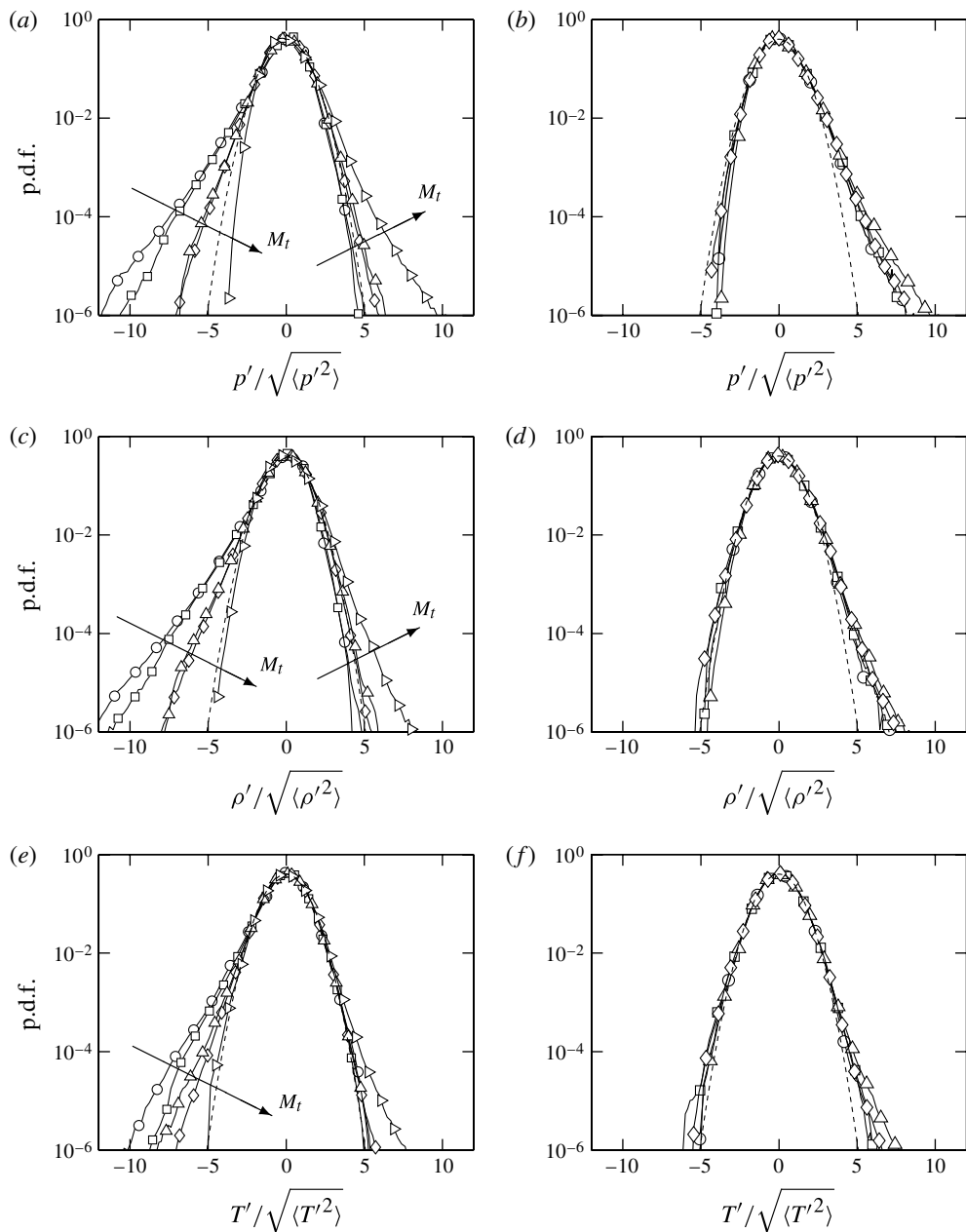


FIGURE 4. Probability density functions of pressure (a,b), density (c,d) and temperature (e,f) fluctuations. (a,c,e) $R_\lambda \approx 100$, and symbols for $M_t \approx 0.1$ (\circ), 0.2 (\square), 0.3 (\diamond), 0.4 (\triangle), and 0.6 (\triangleright). The arrows indicate increasing M_t . (b,d,f) $M_t \approx 0.6$, and the symbols for different Reynolds numbers are as in figure 1. Standard Gaussian distribution (dashed lines) in all plots for comparison.

pressure. The long negative tails in the p.d.f.s in figure 4(a) at low M_t are consistent with high flatness factors. Quantitatively, this is also consistent with incompressible flows (Vedula & Yeung 1999) where F_p is between 5 and 7 at similar Reynolds

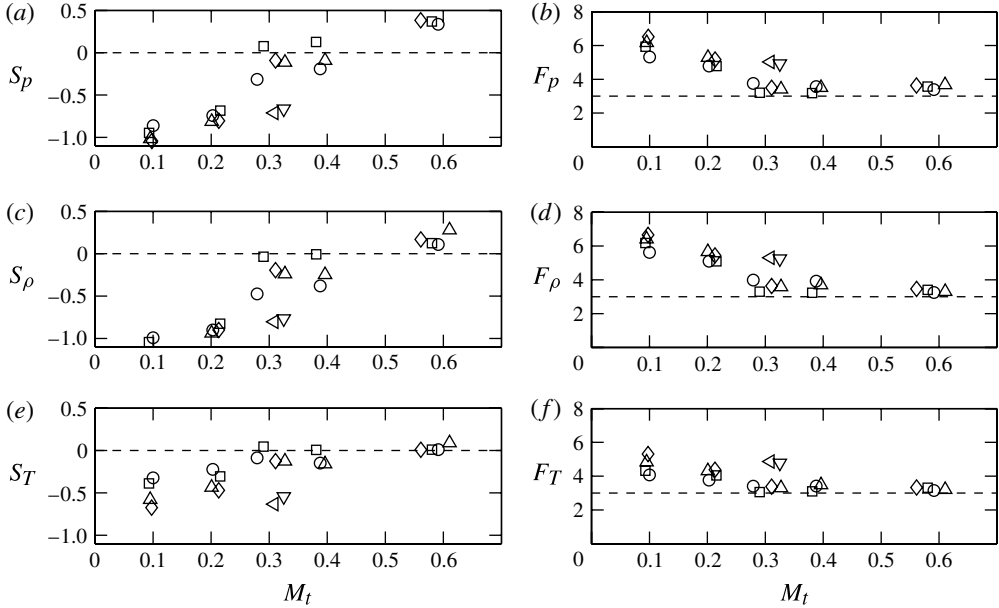


FIGURE 5. Skewness (a,c,e) and flatness (b,d,f) factors for pressure (a,b), density (c,d) and temperature (e,f). The symbols for different Reynolds numbers are as in figure 1.

numbers. At higher M_t , there is a monotonic decrease to values close to 3 (Gaussian). However, since asymmetries in the p.d.f. are also apparent at these Mach numbers (see figure 4b), this is not indicative of Gaussian behaviour.

Density fluctuations present a similar behaviour to that of pressure. This is seen by comparing the p.d.f.s in figure 4(c,d) and skewness and flatness factors in figure 5(c,d) to those for pressure. However, the positive skewness of f_ρ is less pronounced than that of f_p , especially at high M_t . Finally, temperature fluctuations appear to be the least affected by both Reynolds and Mach number effects (figure 4e,f). The skewness and flatness factors for temperature (S_T and F_T) are relatively small in magnitude compared to the counterparts for pressure or density fluctuations (figure 5e,f) and closer to Gaussian.

We note, however, that the comparison of fluctuations in thermodynamic variables to Gaussian statistics has a fundamental limitation. Obviously, as pointed out above, p , ρ and T are positive quantities, which would then require that $p' > -\langle p \rangle$, $\rho' > -\langle \rho \rangle$ and $T' > -\langle T \rangle$. Thus, the p.d.f.s of fluctuations would present, in principle, an asymmetry since their theoretical support would extend from the negative of the mean to (positive) infinity.

While some of the p.d.f.s appear to possess Gaussian characteristics (e.g. the positive tail at low M_t or the negative tail at high M_t), there are reasons to expect density, in particular, to follow log-normal statistics. For example, it can be argued (Blaisdell *et al.* 1993) that, since the continuity equation has a solution of the form $\rho(t) = \rho(0) \exp(-\int_0^t \nabla \cdot \mathbf{u} \, d\tau)$ in Lagrangian coordinates, then for long times, the integral of the divergence of the velocity can be thought of as a sum of independent random variables, each one being the integral over a time-period comparable to the time scale associated with $\nabla \cdot \mathbf{u}$. Invocation of the central limit theorem would then suggest that density is log-normally distributed. Other arguments, including self-similar

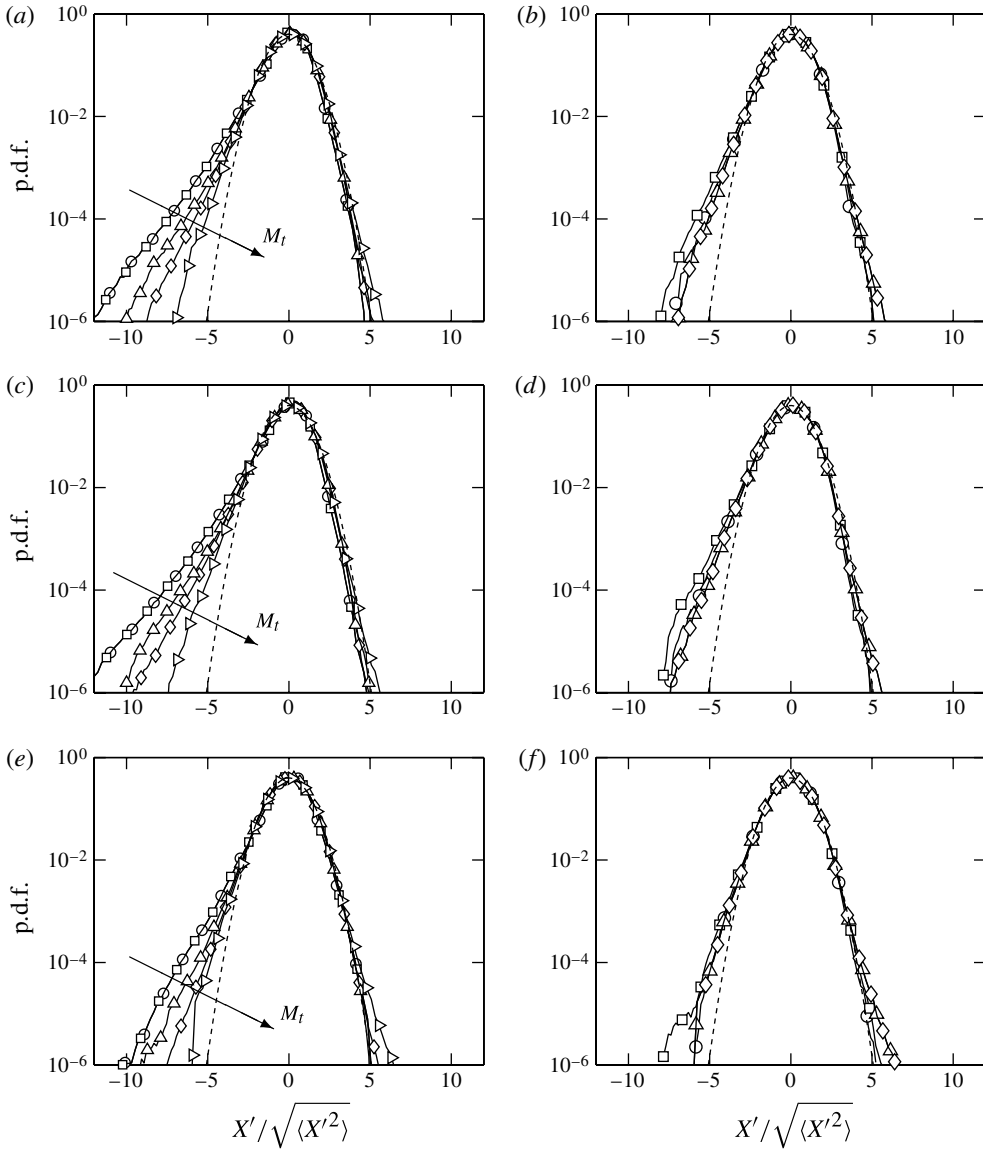


FIGURE 6. Probability density functions of the logarithm of pressure (a,b with $X = \log(p)$), density (c,d with $X = \log(\rho)$) and temperature (e,f with $X = \log(T)$) for the same cases as in figure 4. The arrows indicate increasing M_t . Standard Gaussian distribution (dashed lines) in all plots for comparison.

fragmentation processes similar to those used to understand small-scale intermittency in incompressible flows, have been put forth for isothermal flows, where a log-normal behaviour for density fluctuations has also been observed (e.g. Padoan *et al.* 1997; Federrath *et al.* 2008).

The p.d.f. of the logarithm of density, normalized with its mean and standard deviation, is shown in figure 6(c,d). While negative fluctuations still show a Mach number dependence similar to the p.d.f.s of density itself, positive fluctuations appear

to be very close to log-normal (dashed line). This result appears to be qualitatively consistent with Blaisdell *et al.* (1993), though their data correspond to a sheared flow and was not in a stationary state – statistics were taken only at a single time instant. In contrast, the present data are averaged over many time instants thus improving statistical convergence, especially for the far tails of the p.d.f.s. The negative skewness of the p.d.f. can be intuitively understood (Biskamp 2003) by considering that for $\gamma > 1$, regions with high density will have higher temperatures, and pressure will tend to counteract further compression. If $\gamma < 1$ (when γ is interpreted as a general polytropic exponent), on the other hand, larger values of densities are possible since temperature is reduced in high density regions and the counteracting effect of pressure is much weaker.

While the argument for log-normality above is valid only for density, one can also argue that the other two thermodynamic variables will also be log-normal, under some conditions. As we will see below, positive density and pressure fluctuations appear to be approximately related via an isentropic relation of the form $p \sim \rho^\gamma$. Thus, if density is log-normal with parameters m and s^2 , it is not difficult to show that pressure will also be log-normal with parameters γm and $\gamma^2 s^2$. Similarly, isentropic relations would imply that temperature is related to density via a power law, and we would then expect log-normality for temperature as well. The DNS data appear to support log-normal tails for positive fluctuations of pressure and temperature as seen in figure 6. Negative fluctuations possess wider tails and still retain a Mach number dependence. In particular, as M_t increases, the negative side of the p.d.f.s narrows.

It is not possible to tell from the data whether the entire p.d.f. will approach log-normal behaviour in the high- M_t limit: simulations at higher Mach numbers are required for that purpose. However, one can still argue that this situation may be expected. As M_t increases, more frequent and stronger shock-like structures (shocklets) are expected. Consider the density at a particular location, and a shocklet moving through that location. The change in density during this event $\alpha_0 \equiv \rho_a/\rho_b$ (subscript a and b refer, respectively, to time instants after and before the shock moves through that location) can be calculated according to standard Rankine–Hugoniot relations, for example. Similar considerations apply to expansion-like waves in the turbulence with a corresponding density change. Further, assume that the dominant mechanism for changes in density are due to these shock-like and expansion-like waves. Thus, the density at any instant will be given by $\rho/\rho_0 = \alpha_0\alpha_1\alpha_2, \dots$, where α_i corresponds to the density ratios with i denoting different events and ρ_0 the initial density. We can then take the logarithm to obtain $\log \rho/\rho_0 = \log \alpha_0 + \log \alpha_1 + \log \alpha_2 + \dots$. Finally, if the jumps α_i are statistically independent (which would correspond to the case of randomly distributed shocklets and expansions), the central limit theorem would imply a log-normal behaviour for density. Note that in this case, because expansions and compressions may possess different distributions, the Lindeberg version of the central limit theorem is to be invoked (Feller 1971). Similar arguments can be put forth for the log-normality of pressure and temperature.

It is important to recognize that the preceding argument results in log-normal statistics for the three variables, independent of an isentropic relation between pressure and density, for example. In contrast, the argument in Blaisdell *et al.* (1993) is valid only for density, and log-normality follows if thermodynamic variables are related according to power laws as in isentropic flows.

Since a critical element of this argument is that changes in thermodynamic variables are predominantly due to shock-like or expansion-like events, a log-normal behaviour for the entire distribution will likely be valid only in the high- M_t limit. At moderate

M_t , shocklets are more rare but they may still represent a dominant contribution to large fluctuations. Thus, one may expect the far tails of the p.d.f. to be log-normal, with a core close to Gaussian. The latter can be justified if temperature, for example, behaves as a passive scalar (see § 5) which is known to possess a Gaussian p.d.f. (Mydlarski & Warhaft 1998; Watanabe & Gotoh 2004).

4. The isentropic assumption

In order to simplify theoretical approaches as well as create engineering models, it is often useful to reduce the dependence of any thermodynamic variable from two (§ 1) to one other variable. A widely used approach (at least away from walls or shock waves), though not strictly valid due to the irreversible dissipative nature of turbulence, is to assume that thermodynamic processes occur isentropically (Chandrasekhar 1951; Erlebacher *et al.* 1990). Formally, conservation of energy at constant entropy would imply, with the help of (1.1), that changes in density, pressure, and temperature are related according to

$$p/\langle p \rangle = (\rho/\langle \rho \rangle)^\gamma = (T/\langle T \rangle)^{\frac{\gamma}{\gamma-1}}. \quad (4.1)$$

In this case it is possible to estimate the variance of density and temperature in terms of the variance of pressure. (Note that to first order, this implies that pressure and density fluctuations are related according to $p'/\langle p \rangle \approx \gamma \rho'/\langle \rho \rangle$, Chandrasekhar 1951; Kraichnan 1953). It is easy to rearrange (4.1) to obtain $\rho'^2 = \langle \rho \rangle^2 ((p/\langle p \rangle)^{1/\gamma} - 1)^2$ which can then be expanded as a Taylor series about the mean state. The result is $\rho'^2 \approx (\langle \rho \rangle^2/\gamma^2)(p^*)^2 - (\gamma - 1)(\langle \rho \rangle^2/\gamma^3)(p^*)^3 + O((p^*)^4)$. After taking averages we find that to leading order, $\langle \rho^{*2} \rangle = \langle p^{*2} \rangle/\gamma^2$ or

$$\langle \rho^{*2} \rangle / \langle p^{*2} \rangle = 1/\gamma^2, \quad (4.2)$$

which is also included in figure 3. The DNS data, while in general not far from this prediction, appear to approach $1/\gamma^2$ only at high M_t . A similar calculation for temperature results in

$$\langle T^{*2} \rangle / \langle p^{*2} \rangle = (\gamma - 1)^2/\gamma^2, \quad (4.3)$$

which is seen to be in excellent agreement with DNS data at all M_t . This result is consistent with the weaker M_t dependence observed in the p.d.f. and moments of temperature fluctuations. It is also possible to obtain $2\langle \rho^* T^* \rangle$ by writing the product $\rho' T'$ using the two expressions for density and temperature in (4.1) as a function of pressure. Again, using Taylor series and averaging the result yields, to first order,

$$2\langle \rho^* T^* \rangle / \langle p^{*2} \rangle = 2(\gamma - 1)/\gamma^2. \quad (4.4)$$

As seen in figure 3, this result is also in agreement with DNS data especially at high M_t .

While the ratio of variances appear to follow, at least approximately, relations derived from the isentropic assumption, this does not confirm the fundamental assumption embodied in (4.1), namely, that fluctuations are related as in (4.1) on an instantaneous basis. If this were the case, then the quantity $\beta \equiv (p/\langle p \rangle)/(\rho/\langle \rho \rangle)^\gamma$ would possess a Dirac delta distribution: $f_\beta = \delta(\beta')$ where $\beta' = \beta - \langle \beta \rangle$. In figure 7(a) we show f_β at $R_\lambda \approx 100$ and different Mach numbers. It is clear that while at low M_t the p.d.f. is very narrow, it becomes increasingly wider as M_t increase. At $M_t \approx 0.6$, the p.d.f. is far from a Dirac delta and a range of values of β are observed. In

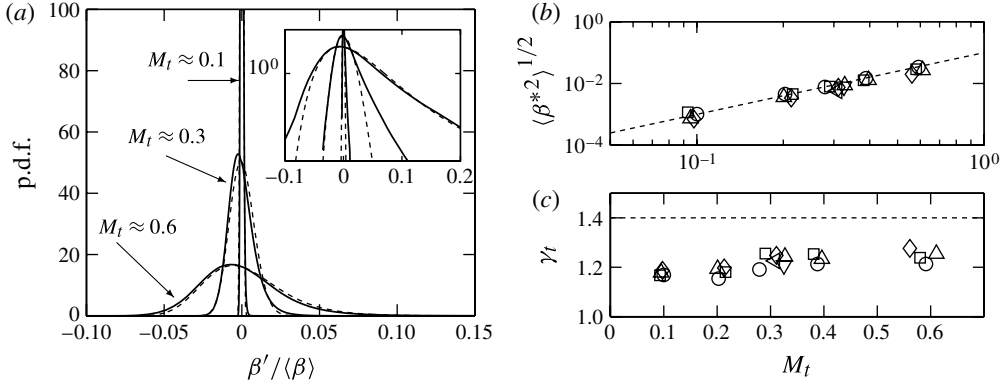


FIGURE 7. (a) Probability density function of $\beta'/\langle\beta\rangle = (\beta - \langle\beta\rangle)/\langle\beta\rangle$ at $R_\lambda \approx 100$ and $M_t \approx 0.1, 0.3$ and 0.6 : dashed lines, (4.6) with best-fit γ_t . The inset shows the same p.d.f.s but with logarithmic scales in the vertical axis. (b) Root mean square of β normalized by its mean: dashed line, $0.1M_t^2$. (c) Effective exponent γ_t . The symbols correspond to different Reynolds numbers as in figure 1.

fact, the r.m.s. of β , which represents a quantitative measure of departures from isentropic behaviour, presents a monotonic growth with M_t . As seen in figure 7(b) this dependence can be well represented by $\langle\beta^{*2}\rangle^{1/2} \equiv \langle(\beta'/\langle\beta\rangle)^2\rangle^{1/2} \approx 0.1M_t^2$ with an imperceptible Reynolds number dependence. We can also see that the most probable value of β shifts to lower values compared to the mean at high M_t . The Reynolds number effect on f_β , as on other p.d.f.s investigated (figure 4), is weak.

Because the p.d.f. of β is not a Dirac delta, fluctuations are not isentropic on an instantaneous basis. However, it may still be possible to link one thermodynamic variable with only one other. A common way to do so is with a polytropic exponent, γ_t , such that

$$p/\langle p \rangle = (\rho/\langle \rho \rangle)^{\gamma_t}. \quad (4.5)$$

Particular cases of interest can be obtained by setting $\gamma_t = \gamma$, $\gamma_t = 1$, or $\gamma_t = 0$, which correspond to isentropic, isothermal and isobaric processes, respectively. Blaisdell *et al.* (1993) argued that this quantity may not be well defined locally (since it is possible to have $\rho' = 0$ while $p' \neq 0$), but that it may still be useful as an approximation in an average sense. The authors in that reference, therefore, used the polytropic exponent defined as $\gamma_t = \sqrt{\langle p^{*2} \rangle / \langle \rho^{*2} \rangle}$ following the first-order approximation of (4.5), $p'/\langle p \rangle = \gamma_t \rho'/\langle \rho \rangle$ suggested by Rubesin (1976). Our objective next is to assess to what degree a polytropic exponent can be defined in a general way to capture fluctuations of all intensities, not just those that provide a dominant contribution to the variance. For this, we turn to the entire p.d.f. of β .

Using (4.5) we can write $\beta = (p/\langle p \rangle)^{(\gamma_t - \gamma)/\gamma_t}$. Clearly, if $\gamma_t = \gamma$, β is always unity. If not, it is still possible to obtain f_β from f_p . Using standard probability concepts (Papoulis & Pillai 2002), we can write $f_\beta(\beta) d\beta = f_p(p) dp$. This implies $f_\beta(\beta) = f_p(\langle p \rangle \beta^{\gamma_t/(\gamma_t - \gamma)}) |dp/d\beta|$ where the derivative is, from the definition of β , $dp/d\beta = \langle p \rangle (\gamma_t/(\gamma_t - \gamma)) (p/\langle p \rangle)^{\gamma_t/\gamma_t}$. A simple yet realistic assumption is that the p.d.f. of p is close to Gaussian. As seen in figure 4(a,b), while inadequate for large fluctuations, it is in fact a good approximation for fluctuations not too far from the

mean. In this case, one obtains

$$f_\beta(\beta) = \frac{\gamma_t}{|\gamma - \gamma_t|} \frac{\beta^{-\frac{\gamma}{\gamma - \gamma_t}}}{\sqrt{2\pi}\langle p^{*2} \rangle^{1/2}} \exp \left[-\frac{1}{2\langle p^{*2} \rangle} \left(\beta^{\frac{\gamma_t}{\gamma - \gamma_t}} - 1 \right)^2 \right], \quad (4.6)$$

where, for a given condition, the only unknown is γ_t which can be found by a best-fit of (4.6) to the DNS data. The result is also shown in figure 7(a). Equation (4.6) seems to provide a good approximation overall, reproducing specific features such as the asymmetry seen from DNS data. The resulting γ_t appears to increase mildly with M_t (figure 7c) though $\gamma_t \approx 1.2$ (which is between isentropic $\gamma_t = 1.4$ and isothermal $\gamma_t = 1$) is a good approximation for the entire range of Reynolds and Mach numbers. The result $1 < \gamma_t < \gamma$ is consistent with the shear flows of Blaisdell *et al.* (1993). A closer look at the p.d.f. in logarithmic scales (inset), however, reveals that the probability of larger fluctuations is underpredicted by (4.6).

We have also obtained f_β using a log-normal distribution for pressure, and similar departures have been observed. This seems to indicate that a single exponent γ_t cannot capture the range of fluctuations in realistic turbulent flows and a relation more complex than (4.5) is necessary. This conclusion is also supported by the fact that the value of γ_t obtained from variances (figure 3 or (4.2) and (4.3)) is different from that obtained from (4.6) aimed at capturing the entire p.d.f.

Regardless of the particular form of $f_p(p)$, since $\beta = (p/\langle p \rangle)^{(\gamma - \gamma_t)/\gamma_t}$, one can expand it using Taylor series as before, square the result and take averages to obtain the root mean square of β which, to leading order, is

$$\langle \beta'^2 \rangle^{1/2} \approx \frac{\gamma - \gamma_t}{\gamma_t} \langle p^{*2} \rangle^{1/2} \approx \frac{\gamma - \gamma_t A \gamma}{\gamma_t} \frac{1}{3} M_t^2. \quad (4.7)$$

Equation (3.5) was used in the last step. We can now see that the departures from pure isentropic fluctuations grow as M_t^2 as the result of the power-law relation between pressure and density and the scaling of pressure variance as in incompressible flows (3.5). Consistency with the best-fit in figure 7(b) requires $\gamma_t \approx 1.2$ (with $A = 1.2$). However, a relation like (4.5) leads to an M_t -independent ratio of variances, identical to those obtained for isentropic fluctuations (with γ_t instead of γ) and presented in figure 3. The conclusion is again that a single exponent does not seem to capture accurately the relation between thermodynamic variables.

Finally, it is of interest to investigate under what conditions non-isentropic effects appear. For this, we have computed the conditional expectation of β given pressure, density and temperature, shown in figure 8 at $R_\lambda \approx 100$. For purely isentropic processes, the conditional expectation would be constant and equal to 1. At $M_t \approx 0.1$ the data are approximately consistent with this result. Interestingly, at higher M_t , a strong asymmetry emerges between positive and negative fluctuations of pressure and density. In particular, while positive fluctuations remain closer to isentropic, negative fluctuations present strong deviations as M_t increases. Large negative fluctuations, however, become more rare as evidenced by the monotonic increase in the skewness of pressure and density. Thus, the competition between stronger fluctuations (intuitively leading to non-isentropic effects) and the shift to positive skewness (leading to positive fluctuations which are more isentropic) may give rise to more complex behaviour such as seemingly isentropic fluctuations at high M_t , as has indeed been observed in figure 3. Further investigations are required in this direction.

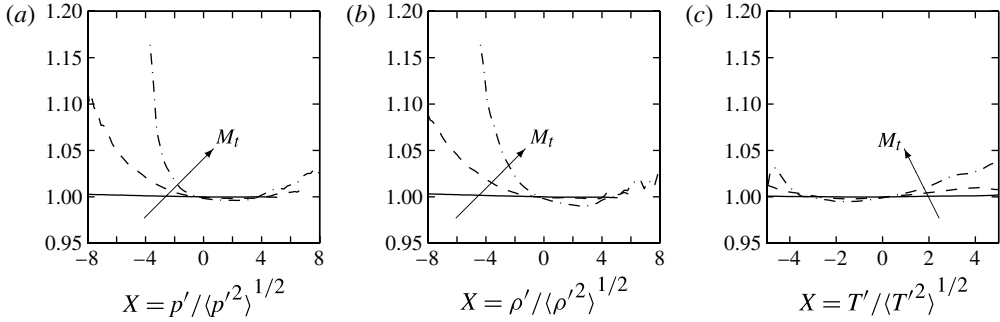


FIGURE 8. Conditional expectations $\langle \beta / \langle \beta \rangle | X \rangle$ with $X = p' / \langle p'^2 \rangle^{1/2}$ (a), $X = \rho' / \langle \rho'^2 \rangle^{1/2}$ (b), and $X = T' / \langle T'^2 \rangle^{1/2}$ (c) at $R_\lambda \approx 100$ and $M_t \approx 0.1$ (solid), 0.3 (dashed), and 0.6 (dot-dashed). The arrows indicate increasing M_t .

5. Spectra of thermodynamic variables

At low M_t , compressible turbulence is expected to possess characteristics similar to its incompressible counterpart. For example, as indicated in §3, the p.d.f. of pressure at $M_t \approx 0.1$ is consistent with incompressible results in the literature. Another well-known result for incompressible turbulence is the spectrum of pressure (Monin & Yaglom 1975), which according to the classical theory of Kolmogorov (1941) presents a universal form for wavenumbers $k \gg 1/L$ (L is the integral length scale):

$$E_p(k) = C_p \langle \epsilon \rangle^{3/4} \nu^{7/4} f(k\eta), \quad (5.1)$$

where $\langle \epsilon \rangle$ is the average energy dissipation rate and C_p is a constant of order one. In the inertial range ($1/L \ll k \ll 1/\eta$ where $\eta \equiv (\nu^3/\langle \epsilon \rangle)^{1/4}$ is the Kolmogorov length scale) it is expected that $f(k\eta) \rightarrow (k\eta)^{-7/3}$, and the pressure spectrum assumes the form

$$E_p(k) = C_p \langle \epsilon \rangle^{4/3} k^{-7/3}. \quad (5.2)$$

In figure 9(a) we show the compensated pressure spectrum according to (5.2) (such that inertial-range scaling would appear as a plateau at intermediate scales) for $M_t \approx 0.1$ and different Reynolds numbers. As expected, the data appear to possess the universality observed at high wavenumbers in incompressible flows with an emerging inertial-range scaling as R_λ increases. While one may be tempted to read the value of C_p from the maximum seen at $k\eta \approx 0.2$, this may not be entirely justified if, as with the kinetic energy spectrum, a spectral bump emerges at the end of the inertial range. This has indeed been responsible for overestimations of the Kolmogorov constant for the energy spectrum in earlier DNS (Donzis, Sreenivasan & Yeung 2010). The situation is clearly seen in figure 10(a), where we show the compensated energy spectrum according to the classical $E(k) = C_K \langle \epsilon \rangle^{2/3} k^{-5/3}$ in the inertial range (Kolmogorov 1941). The inertial range is seen as a plateau at intermediate wavenumbers followed by a spectral bump (bottleneck) with a maximum around $k\eta \approx 0.1$. The dashed line at $C_K = 1.6$ corresponds to the value obtained from incompressible flows (Donzis *et al.* 2010). In general, the energy spectra from our compressible simulations shown in figure 10, are entirely consistent with incompressible results in the literature. No inertial-range scaling can be unambiguously observed for R_λ below 100. Mach number effects are imperceptible, though they are likely to increase at higher M_t .

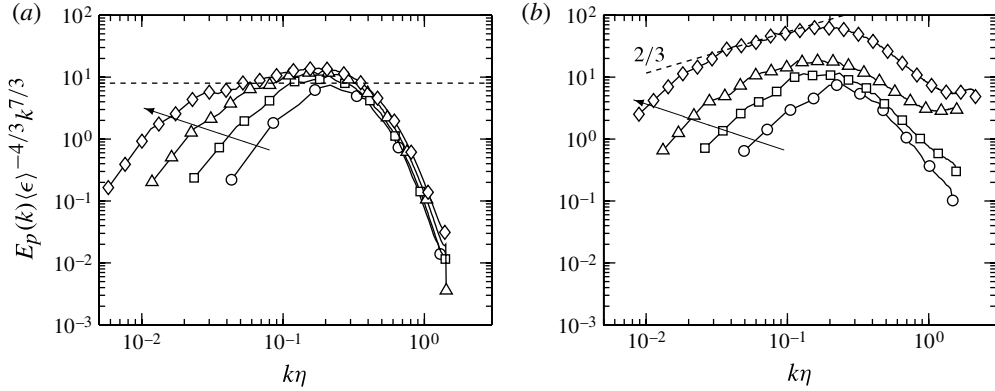


FIGURE 9. (a) Normalized pressure spectrum for $R_\lambda \approx 38, 60, 100, 170$ at $M_t \approx 0.1$. Horizontal dashed line at $C_p = 8$ (Gotoh & Fukayama 2001). (b) The same data but at $M_t \approx 0.6$. The dashed line with slope $2/3$ corresponds to $k^{-5/3}$ for $E_p(k)$ in the present normalization. The symbols for different Reynolds numbers are as in figure 1. The arrows indicate increasing R_λ .

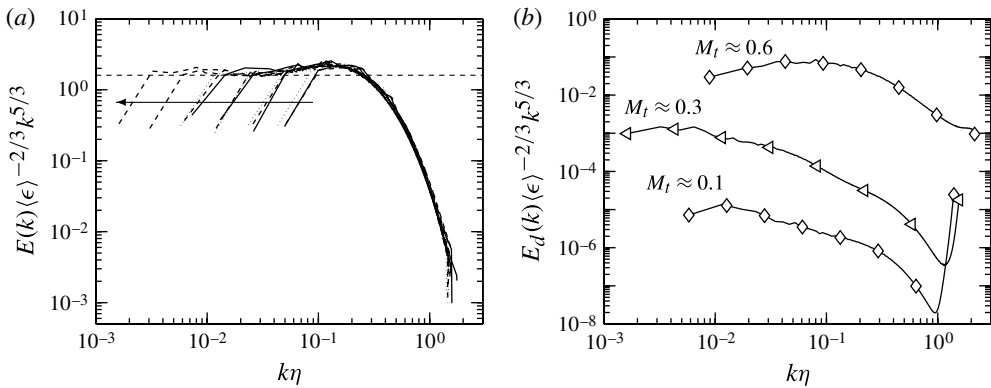


FIGURE 10. (a) Normalized energy spectrum for $R_\lambda \approx 38, 60, 100, 170, 270$ and 430 at $M_t \approx 0.1$ (solid), 0.3 (dashed) and 0.6 (dotted). The arrow indicates increasing R_λ . Horizontal dashed line at $C_K = 1.6$ (Donzis *et al.* 2010). (b) Normalized dilatational energy spectrum for $M_t \approx 0.1, 0.3$ and 0.6 at the highest R_λ available for each case (i.e. $170, 430$ and 170 , respectively). The symbols for different Reynolds numbers are as in figure 1.

For reference we also present in figure 10(b) the dilatational spectrum $E_d(k)$ obtained from the irrotational or dilatational component of a Helmholtz decomposition of the velocity field (e.g. Kida & Orszag 1990) for $M_t \approx 0.1, 0.3$ and 0.6 at the highest R_λ available for each case. While inertial-range scaling is difficult to observe, we note that the energy in the dilatational component is orders of magnitude smaller than the total energy, though its contribution grows with M_t . This is consistent with the data in table 1. We note that at very high wavenumbers ($k\eta > 1$) some well-known residual errors (e.g. Watanabe & Gotoh 2007; Ishihara, Gotoh & Kaneda 2009) are seen, though their contribution to total energy is negligible (the effect is greatly amplified in

the figure by the multiplication by $k^{5/3}$ due to the normalization) and have virtually no effect on the quantities of interest here.

The spectral bump at the end of the inertial range has also been observed in the pressure spectrum around $k\eta \approx 0.1\text{--}0.2$ (Gotoh & Fukayama 2001), consistent with our results in figure 9(a). However, the appearance of a $k^{-7/3}$ scaling range is apparent only at R_λ beyond $\sim 400\text{--}600$ (Gotoh & Fukayama 2001; Tsuji & Ishihara 2003). We also include a horizontal line corresponding to $C_p = 8.0$ which would mark the expected inertial-range scaling at higher Reynolds numbers in incompressible turbulence (Gotoh & Fukayama 2001). Higher Reynolds numbers are clearly needed to establish conclusively the appearance of $k^{-7/3}$.

While we have observed similar results at $M_t \lesssim 0.3\text{--}0.4$, a different picture emerges at higher M_t . In figure 9(b) we show the same normalized pressure spectrum at $M_t \approx 0.6$, where it is clear that incompressible scaling is inadequate. This may not be surprising. As mentioned in § 3, at $M_t \approx 0.6$ the variance of ‘compressible’ pressure is of the same order as that for the ‘incompressible’ pressure and it is only the latter which may be expected to follow incompressible scaling. If the former does not scale as suggested by (5.1), then an increase in Reynolds number (through a decrease in viscosity, for example) would imply a smaller denominator in the normalized spectrum $E_p / \langle \epsilon \rangle^{3/4} \nu^{7/4}$ and an increase in spectral levels at all wavenumbers, which is what is observed in the figure. We have indeed observed that the spectrum of the ‘compressible’ pressure resembles closely the behaviour seen in figure 9(b) and is therefore not shown.

It may thus be natural to expect the scaling of the pressure spectrum to be increasingly influenced by thermodynamics instead of the classical hydrodynamic processes in the inertial range as M_t increases. It is also interesting to observe that, at high M_t , as the Reynolds numbers increases a scaling range develops with a slope shallower than $-7/3$. In fact, at the highest R_λ available for $M_t \approx 0.6$, the pressure spectrum appears to have a $k^{-5/3}$ scaling in the inertial range (the dashed line in figure 9(b)). While $k^{-5/3}$ has been reported for the pressure spectrum in earlier DNS of incompressible turbulence (Cao *et al.* 1999; Gotoh & Rogallo 1999; Vedula & Yeung 1999), Gotoh & Fukayama (2001) showed that due to the low Reynolds numbers, the inertial range scaling was confused with the spectral bump. From figure 9(b) it is clear that the scaling region emerges at wavenumbers lower than that corresponding to the bottleneck and is therefore considered true inertial-range scaling. As we discuss next, a $k^{-5/3}$ may not be completely unexpected.

For low Mach numbers, it is expected that temperature would behave as a passive scalar. This is easily seen if the energy equation is written in terms of temperature (in our perfect gas model $T = e/C_v$, where e is the internal energy per unit mass and C_v the specific heat at constant volume). If fluctuations of thermodynamic quantities are small, then one can expect fluctuations in molecular diffusivities to be small as well. The resulting equation under these assumptions is a forced advection–diffusion equation for T with the thermal diffusivity given by $\alpha = \kappa/\rho C_v$ (κ is the thermal conductivity and density, as a first approximation, can be taken as its mean value) and source terms of different types (mainly viscous dissipation and pressure–dilatation correlation).

The problem of turbulent mixing governed by this type of advection–diffusion equation has been studied extensively (Warhaft 2000). For scalars with diffusivities of the order of, or larger than, the diffusivity of momentum (that is, Schmidt or Prandtl numbers of order one or less, which is the case in our simulations), Obukhov (1949) and Corrsin (1951) extended the theory of Kolmogorov (1941) with a cascade of scalar

fluctuations similar to the classical energy cascade for the velocity field (Monin & Yaglom 1975). Scalar fluctuations are injected or produced at the large scalar scales, and through successive breakdowns into ever smaller scales the cascade proceeds until fluctuations are ultimately dissipated at the smallest scalar scales. The average rate at which the scalar (in our case temperature) fluctuations are destroyed by the effect of diffusivity is readily found to be $\langle \epsilon_T \rangle \equiv 2\alpha \langle (\nabla T')^2 \rangle$. During this step-by-step process the details of the large scales and how the fluctuations were generated by the flow becomes weaker; the small scales, then, are believed to acquire an increasingly isotropic and universal character.

In this picture, there is an intermediate range of scales (between the largest scalar scales and the smallest diffusive scales), the so-called inertial-convective range, in which the dynamics is not affected by either the production mechanisms (large scales), or the viscous and diffusive processes (small scales). The scalar spectrum in the inertial-convective range is then given by (Monin & Yaglom 1975)

$$E_T(k) = C_{OC}^T \langle \epsilon \rangle^{-1/3} \langle \epsilon_T \rangle k^{-5/3}, \quad (5.3)$$

where C_{OC}^T is the Obukhov–Corrsin constant for temperature fluctuations. Whereas, as argued above, high Reynolds numbers are needed to observe a true inertial range in the velocity field, an inertial-convective range for scalars is known to emerge at lower Reynolds numbers than for the velocity field (Sreenivasan 1996; Yeung, Donzis & Sreenivasan 2005; Donzis *et al.* 2010; Lee *et al.* 2012).

In figure 11(a) we show the compensated temperature spectrum $E_T(k)$ according to (5.3) at $M_t \approx 0.1$. The collapse of temperature spectra at high wavenumbers reflects the universality at small scales predicted by the incompressible theory. As R_λ increases, we see the usual widening of the inertial-convective range towards lower wavenumbers. At the highest R_λ , inertial-convective scaling is already apparent as a plateau at intermediate scales. Although the Obukhov–Corrsin constant read from the figure ($C_{OC}^T \approx 1.1$) appears to be somewhat higher than that for incompressible flows (Watanabe & Gotoh 2004), in general, our results are consistent with them.

Qualitatively similar results are observed at higher Mach numbers. In figure 11(b) we show the temperature spectrum at $M_t \approx 0.6$. The main effect of increasing M_t appears to be confined at low wavenumbers. This increase of spectral levels at low wavenumbers is consistent with the temperature variance growing with M_t (figure 2c) because the variance of temperature is the integral of the spectrum (Parseval's theorem) and the dominant contribution is from low wavenumber modes. While small scales appear to preserve Obukhov–Corrsin scaling, the increase of spectral levels at lower wavenumbers results in a slight increase in C_{OC}^T with the Mach number. However, it is plausible that this effect will disappear at even higher Reynolds numbers, where the inertial range widens and the effect of large scales on inertial and diffusive scales is expected to weaken.

The density spectrum has been studied in different contexts, though perhaps more thoroughly in astrophysics. A number of authors have suggested a $k^{-5/3}$ spectrum based on different sets of assumptions and conditions, which include weakly compressible flows, magnetohydrodynamic turbulence, and the interstellar medium (e.g. Montgomery, Brown & Matthaeus 1987; Bayly, Levermore & Passot 1992; Dastgeer & Zank 2005; Hunana & Zank 2010). Many of these studies, however, have focused on isothermal turbulence, which makes the applicability of their results problematic in our context. An alternative $k^{-7/3}$ has also been suggested under certain conditions based on the similarity between pressure and density (Bayly *et al.* 1992).

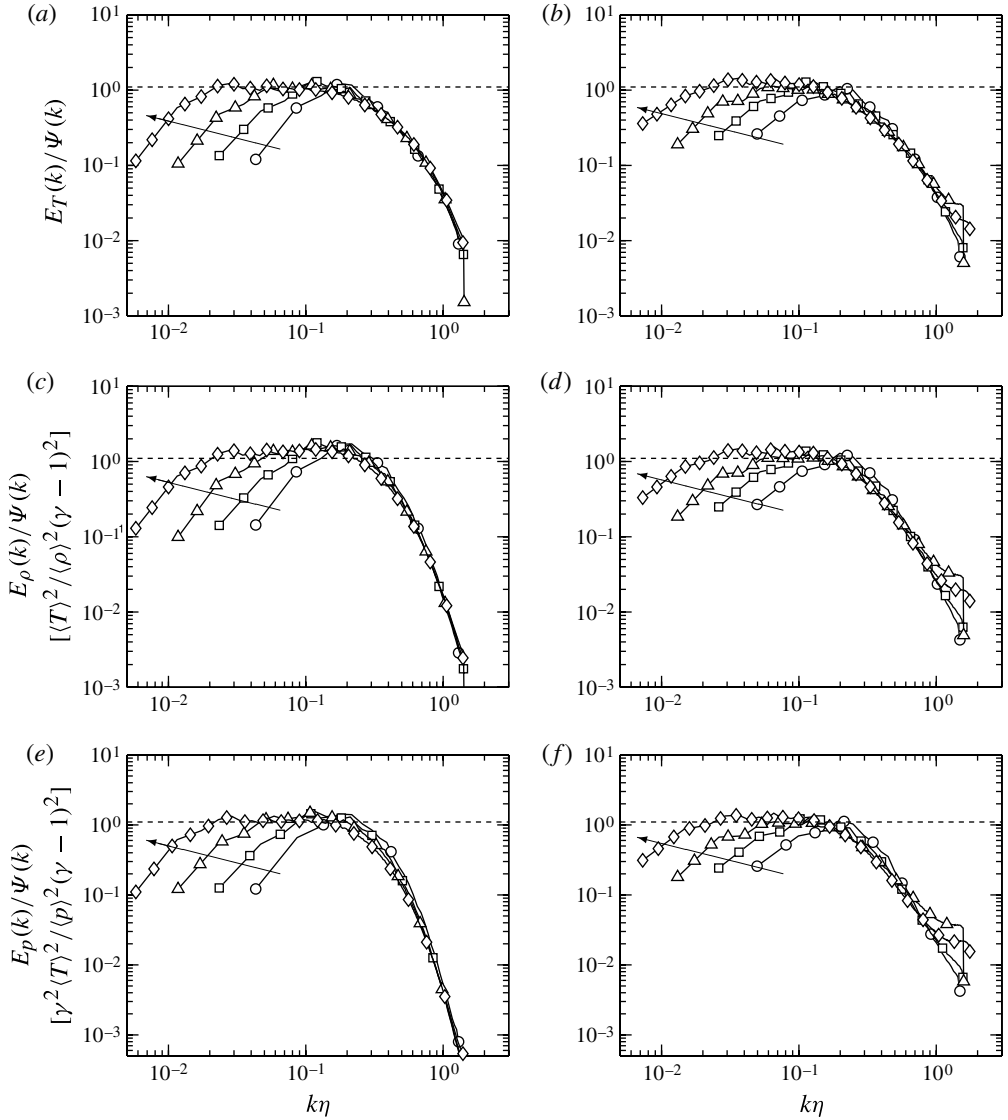


FIGURE 11. Spectrum of temperature (*a,b*), density (*c,d*), and pressure (*e,f*) at $M_t \approx 0.1$ (*a,c,e*) and 0.6 (*b,d,f*) compensated according to (5.3), (5.5) and (5.6), respectively. To simplify notation we define $\Psi(k) \equiv \langle \epsilon \rangle^{-1/3} \langle \epsilon_T \rangle k^{-5/3}$. The symbols for different Reynolds numbers are as in figure 1. The arrows indicate increasing R_λ .

Although, as argued in §4, large fluctuations depart from isentropic behaviour, figure 8 also shows that moderate fluctuations may not be too far from isentropic. Thus, even though estimation of high-order moments of thermodynamic variables will probably be inaccurate if pure isentropic processes are assumed, second-order statistics (including the spectrum) may still be accurately predicted. In this case, according to (4.1), density and temperature fluctuations are related according to $\rho'/\rho \approx (\gamma - 1)^{-1} T'/T$ to first order. Therefore, the density spectrum can be written

in terms of the temperature spectrum as

$$E_\rho(k) = \frac{\langle \rho \rangle^2}{\langle T \rangle^2} \frac{1}{(\gamma - 1)^2} E_T(k). \quad (5.4)$$

In the inertial-convective range, in particular, we can use (5.3) to obtain

$$E_\rho(k) = C_{OC}^T \frac{\langle \rho \rangle^2}{\langle T \rangle^2} \frac{1}{(\gamma - 1)^2} \langle \epsilon \rangle^{-1/3} \langle \epsilon_T \rangle k^{-5/3}. \quad (5.5)$$

In figure 11(c) we show the density spectrum compensated according to (5.5). There is an excellent collapse of $E_\rho(k)$ at high wavenumbers and a $k^{-5/3}$ inertial-convective scaling is also apparent at the highest Reynolds number. The horizontal dashed line corresponds to C_{OC}^T , which is seen to be slightly below the DNS data. Note that this difference may be absorbed in (5.5) if a general polytropic process (4.5) is assumed – the resulting expression would be the same equation (5.5), but with γ_t instead of γ . In fact, a better agreement with the DNS data are obtained with $\gamma_t < \gamma$, which is also consistent with the results based on single-point statistics in § 3. Figure 11(d) shows the same compensated density spectrum at $M_t \approx 0.6$. Mach number effects at low wavenumbers are seen to be qualitatively similar to those for the temperature spectrum.

Under the same isentropic assumption, pressure and temperature fluctuations are related as $p' \approx \langle p \rangle / \langle T \rangle \gamma (\gamma - 1)^{-1} T'$, which thus yields

$$E_p(k) = C_{OC}^T \frac{\langle p \rangle^2}{\langle T \rangle^2} \frac{\gamma^2}{(\gamma - 1)^2} \langle \epsilon \rangle^{-1/3} \langle \epsilon_T \rangle k^{-5/3}. \quad (5.6)$$

Figure 11(e,f) shows the compensated spectrum for pressure according to (5.6). Just as for density there is a good collapse of the DNS data at both low and high M_t .

It is important to note that while a $k^{-5/3}$ scaling for temperature may indicate a spectral cascade similar to passive scalars in incompressible turbulence, this conclusion can be justified only by the similarity of the governing equations. This, however, is not the case for density and pressure. The $k^{-5/3}$ observed for $E_\rho(k)$ and $E_p(k)$ appears to be the result of the linearized relation with temperature and thus does not immediately imply a classical spectral cascade of density and pressure due to nonlinear interactions of different scales.

We conclude this section by noting that even though the different spectra appear to follow $k^{-5/3}$ in the inertial range, simulations at higher Reynolds numbers with a wider range of scales are desired to provide a more accurate assessment of the spectral slope, especially if small intermittency corrections in the inertial range (Sreenivasan & Antonia 1997) are sought. This seems to be more important for pressure fluctuations for which it is not possible, without some ambiguity, to rule out $k^{-7/3}$ at low M_t . We also note that at the highest Mach number (figure 11b,d,f) the so-called dissipative range ($k\eta \gtrsim 0.2$) appears to possess higher spectral content than at low M_t , especially for density and pressure. This may be indicative of the effect of small-scale features such as shocklets, and its detailed investigation is deferred to a future publication.

6. Conclusion

Using a large DNS database of forced compressible turbulence we have investigated the scaling of pressure, density and temperature fluctuations in an ideal gas. Variances of thermodynamic variables grow with M_t as a power law steeper than 4 (the exponent

that results from a direct extension of the known incompressible scaling of pressure variance with the velocity variance, to compressible flows). The covariance between density and temperature is a non-negligible contribution to the scaling of both the mean as well as the variance of pressure. Temperature fluctuations are in general smaller and less correlated to the other two quantities. While results at low M_t are consistent with incompressible results, qualitative changes are observed at high M_t . For example, the skewness of pressure and density changes from negative values to positive with a transition between $M_t \approx 0.3$ and 0.4 . At low M_t , the p.d.f. of pressure is consistent with incompressible results: a long negative tail and a positive tail close to Gaussian. As M_t increases, the negative side narrows and the positive side widens. A possible explanation is the increase in the amplitude of pressure fluctuations combined with the positiveness of pressure which bounds fluctuations from below. Similar conclusions apply to density and temperature.

We have further investigated a suggestion in the literature that density should obey log-normal statistics. We found that while positive fluctuations are well approximated by a log-normal distribution independent of R_λ and M_t , negative fluctuations still retain an M_t effect similar to that observed in the p.d.f. of the variables themselves. We argued that if one variable is log-normal, a polytropic relation will imply log-normality for all of them. We have also discussed a physical mechanism leading to log-normal statistics for all thermodynamic variables which does not rely on the assumption of polytropic processes. The key element in the argument is the dominance of compression and expansion waves randomly passing through a point, which, via a central limit argument, results in a random process with log-normal statistics.

We have also investigated the extent to which fluctuations can be assumed to be isentropic. Although some results can be approximated using isentropic relations, departures from purely isentropic processes grow as M_t^2 (measured by the variance of β). Positive pressure and density fluctuations tend to be more isentropic than negative fluctuations. An alternative polytropic exponent was investigated and the results suggest that a single exponent cannot represent fluctuations of all intensities. In general, all our results indicate that Reynolds number effects are weak for single-point statistics.

The DNS database has also been used to address the scaling of pressure, density and temperature spectra. While spectra for the three thermodynamic variables of interest here are consistent with a $k^{-5/3}$ inertial range scaling, the pressure spectrum may also be consistent with $k^{-7/3}$ at low M_t , following known results in incompressible turbulence. The $k^{-5/3}$ scaling can be expected if temperature behaves as a passive scalar and fluctuations of density and pressure are proportional to temperature, an approximation valid for small fluctuations under a general polytropic relation (including isentropic) between variables. An unambiguous determination of inertial-range scaling will require even higher Reynolds numbers and resolutions.

Acknowledgements

The authors acknowledge support from NSF (grant OCI-1054966) and AFOSR (grant FA9550-12-1-0168). We used computational resources at TACC (University of Texas at Austin) and NICS (University of Tennessee) through the Extreme Science and Engineering Discovery Environment (XSEDE), as well as at Oak Ridge and Argonne National Laboratories.

REFERENCES

- BAYLY, B. J., LEVERMORE, C. D. & PASSOT, T. 1992 Density variations in weakly compressible flows. *Phys. Fluids* **4**, 945–954.
- BEETZ, C., SCHWARZ, C., DREHER, J. & GRAUER, R. 2008 Density-PDFs and Lagrangian statistics of highly compressible turbulence. *Phys. Lett. A* **372**, 3037–3041.
- BISKAMP, D. 2003 *Magnetohydrodynamic Turbulence*. Cambridge University Press.
- BLAISDELL, G. A., MANSOUR, N. N. & REYNOLDS, W. C. 1993 Compressibility effects on the growth and structure of homogeneous turbulent shear flow. *J. Fluid Mech.* **256**, 443–485.
- CAO, N. Z., CHEN, S. Y. & DOOLEN, G. D. 1999 Statistics and structures of pressure in isotropic turbulence. *Phys. Fluids* **11**, 2235–2250.
- CHANDRASEKHAR, S. 1951 The fluctuations of density in isotropic turbulence. *Proc. R. Soc. Lond. A* **210** (1100), 18–25.
- CORRSIN, S. 1951 On the spectrum of isotropic temperature fluctuations in an isotropic turbulence. *J. Appl. Phys.* **22**, 469–473.
- DASTGEER, S. & ZANK, G. P. 2005 Turbulence in nearly incompressible fluids: density spectrum, flows, correlations and implication to the interstellar medium. *Nonlinear Proc. Geophys.* **12**, 139–148.
- DENBIGH, K. 1981 *The Principles of Chemical Equilibrium*. Cambridge University Press.
- DONZIS, D. A. & SREENIVASAN, K. R. 2010 The bottleneck effect and the Kolmogorov constant in isotropic turbulence. *J. Fluid Mech.* **657**, 171–188.
- DONZIS, D. A., SREENIVASAN, K. R. & YEUNG, P. K. 2010 The Batchelor spectrum for mixing of passive scalars in isotropic turbulence. *Flow Turbul. Combust.* **85**, 549–566.
- DONZIS, D. A., SREENIVASAN, K. R. & YEUNG, P. K. 2012 Some results on the Reynolds number scaling of pressure statistics in isotropic turbulence. *Physica D* **241**, 164–168.
- ERLEBACHER, G., HUSSAINI, M. Y., KREISS, H. O. & SARKAR, S. 1990 The analysis and simulation of compressible turbulence. *Theor. Comput. Fluid Dyn.* **2**, 73–95.
- ESWARAN, V. & POPE, S. B. 1988 An examination of forcing in direct numerical simulations of turbulence. *Comput. Fluids* **16**, 257–278.
- FEDERRATH, C., KLESSEN, R. S. & SCHMIDT, W. 2008 The density probability distribution in compressible isothermal turbulence: solenoidal versus compressive forcing. *Astrophys. J. Lett.* **688**, L79–L82.
- FELLER, W. 1971 *An Introduction to Probability Theory and its Applications*. Wiley.
- GOTOH, T. & FUKAYAMA, D. 2001 Pressure spectrum in homogeneous turbulence. *Phys. Rev. Lett.* **86**, 3775–3778.
- GOTOH, T. & ROGALLO, R. S. 1999 Intermittency and scaling of pressure at small scales in forced isotropic turbulence. *J. Fluid Mech.* **396**, 257–285.
- HUNANA, P. & ZANK, G. P. 2010 Inhomogeneous nearly incompressible description of magnetohydrodynamic turbulence. *Astrophys. J.* **718**, 148–167.
- ISHIHARA, T., GOTOH, T. & KANEDA, Y. 2009 Study of high-Reynolds number isotropic turbulence by direct numerical simulation. *Annu. Rev. Fluid Mech.* **41**, 165–180.
- JAGANNATHAN, S. & DONZIS, D. A. 2012 Massively parallel direct numerical simulations of forced compressible turbulence: a hybrid MPI/OpenMP approach. In *Proceedings of the 1st Conference of the Extreme Science and Engineering Discovery Environment*, p. 23.
- KIDA, S. & ORSZAG, S. A. 1990 Energy and spectral dynamics in forced compressible turbulence. *J. Sci. Comp.* **5**, 85–125.
- KIDA, S. & ORSZAG, S. A. 1992 Energy and spectral dynamics in decaying compressible turbulence. *J. Sci. Comp.* **7**, 1–34.
- KOLMOGOROV, A. N. 1941 Local structure of turbulence in an incompressible fluid for very large Reynolds numbers. *Dokl. Akad. Nauk SSSR* **30**, 299–303.
- KRAICHNAN, R. H. 1953 The scattering of sound in a turbulent medium. *J. Acoust. Soc. Am.* **25**, 1096–1104.
- LEE, S. K., BENAÏSSA, A., DJENIDI, L., LAVOIE, P. & ANTONIA, R. A. 2012 Scaling range of velocity and passive scalar spectra in grid turbulence. *Phys. Fluids* **24**, 075101.
- LEE, K. & GIRIMAJI, S. 2011 Flow–thermodynamics interactions in decaying anisotropic compressible turbulence with imposed temperature fluctuations. In *Theor. Comput. Fluid Dyn.*, pp. 1–17.

- LEE, S., LELE, S. K. & MOIN, P. 1991 Eddy shocklets in decaying compressible turbulence. *Phys. Fluids* **3**, 657–664.
- LELE, S. K. 1994 Compressibility effects on turbulence. *Annu. Rev. Fluid Mech.* **26**, 211–254.
- MONIN, A. S. & YAGLOM, A. M. 1975 *Statistical Fluid Mechanics*, vol. II, MIT.
- MONTGOMERY, D., BROWN, M. R. & MATTHAEUS, W. H. 1987 Density fluctuation spectra in magnetohydrodynamic turbulence. *J. Geophys. Res.* **92**, 282–284.
- MYDLARSKI, L. & WARHAFT, Z. 1998 Passive scalar statistics in high-Peclet-number grid turbulence. *J. Fluid Mech.* **358**, 135–175.
- OBUKHOV, A. M. 1949 The structure of the temperature field in a turbulent flow. *Izv. Akad. Nauk SSSR* **13**, 58–69.
- PADOAN, P., JONES, B. J. T. & NORDLUND, A. P. 1997 Supersonic turbulence in the interstellar medium: stellar extinction determinations as probes of the structure and dynamics of dark clouds. *Astrophys. J.* **474**, 730–734.
- PAPOULIS, A. & PILLAI, S. U. 2002 *Probability, Random Variables and Stochastic Processes*, 4th edn. McGraw-Hill.
- PETERSEN, M. R. & LIVESCU, D. 2010 Forcing for statistically stationary compressible isotropic turbulence. *Phys. Fluids* **22**, 116101.
- PIROZZOLI, S. 2011 Numerical methods for high-speed flows. *Annu. Rev. Fluid Mech.* **43**, 163–194.
- PIROZZOLI, S. & GRASSO, F. 2004 Direct numerical simulations of isotropic compressible turbulence: influence of compressibility on dynamics and structures. *Phys. Fluids* **16**, 4386–4407.
- PUMIR, A. 1994 A numerical study of pressure-fluctuations in three-dimensional, incompressible, homogeneous, isotropic turbulence. *Phys. Fluids* **6**, 2071–2083.
- RUBESIN, M. W. 1976 A one-equation model of turbulence for use with the compressible Navier–Stokes equations. NASA Tech. Memo. X-73128.
- SAMTANEY, R., PULLIN, D. I. & KOSOVIC, B. 2001 Direct numerical simulation of decaying compressible turbulence and shocklet statistics. *Phys. Fluids* **13**, 1415–1430.
- SARKAR, S., ERLEBACHER, G., HUSSAINI, M. Y. & KREISS, H. O. 1991 The analysis and modelling of dilatational terms in compressible turbulence. *J. Fluid Mech.* **227**, 473–493.
- SCALO, J., VÁZQUEZ-SEMADENI, E., CHAPPELL, D. & PASSOT, T. 1998 On the probability density function of galactic gas. Part 1. Numerical simulations and the significance of the polytropic index. *Astrophys. J.* **504**, 835–853.
- SMITS, A. J. & DUSSAUGE, J. P. 2006 *Turbulent Shear Layers in Supersonic Flow*. Springer.
- SREENIVASAN, K. R. 1996 The passive scalar spectrum and the Obukhov–Corrsin constant. *Phys. Fluids* **8**, 189–196.
- SREENIVASAN, K. R. & ANTONIA, R. A. 1997 The phenomenology of small-scale turbulence. *Annu. Rev. Fluid Mech.* **29**, 435–472.
- TSUJI, Y. & ISHIHARA, T. 2003 Similarity scaling of pressure fluctuation in turbulence. *Phys. Rev. E* **68**, 026309.
- VEDULA, P. & YEUNG, P. K. 1999 Similarity scaling of acceleration and pressure statistics in numerical simulations of isotropic turbulence. *Phys. Fluids* **11**, 1208–1220.
- WANG, J., SHI, Y., WANG, L.-P., XIAO, Z., HE, X. & CHEN, S. 2011 Effect of shocklets on the velocity gradients in highly compressible isotropic turbulence. *Phys. Fluids* **23**, 125103.
- WANG, J., SHI, Y., WANG, L.-P., XIAO, Z., HE, X. T. & CHEN, S. 2012 Effect of compressibility on the small-scale structures in isotropic turbulence. *J. Fluid Mech.* **713**, 588–631.
- WARHAFT, Z. 2000 Passive scalars in turbulent flows. *Annu. Rev. Fluid Mech.* **32**, 203–240.
- WATANABE, T. & GOTOH, T. 2004 Statistics of a passive scalar in homogeneous turbulence. *New J. Phys.* **6**, 40.
- WATANABE, T. & GOTOH, T. 2007 Inertial-range intermittency and accuracy of direct numerical simulation for turbulence and passive scalar turbulence. *J. Fluid Mech.* **590**, 117–146.
- YEUNG, P. K., DONZIS, D. A. & SREENIVASAN, K. R. 2005 High-Reynolds-number simulation of turbulent mixing. *Phys. Fluids* **17**, 081703.